Pulsed, single-mode cavity ringdown spectroscopy

Roger D. van Zee, Joseph T. Hodges, and J. Patrick Looney

We discuss the use of single-mode cavity ringdown spectroscopy with pulsed lasers for quantitative gas density and line strength measurements. The single-mode approach to cavity ringdown spectroscopy gives single exponential decay signals without mode beating, which allows measurements with uncertainties near the shot-noise limit. The technique is demonstrated with a 10-cm-long ringdown cavity and a pulsed, frequency-stabilized optical parametric oscillator as the light source. A noise-equivalent absorption coefficient of 5×10^{-10} cm^{-1} Hz$^{-1/2}$ is demonstrated, and the relative standard deviation in the ringdown time (σ_τ/τ) extracted from a fit to an individual ringdown curve is found to be the same as that for an ensemble of hundreds of independent measurements. Repeated measurement of a line strength is shown to have a standard deviation $<0.3\%$. The effects of normally distributed noise on quantities measured using cavity ringdown spectroscopy are discussed, formulas for the relative standard deviation in the ringdown time are given in the shot- and technical-noise limits, and the noise-equivalent absorption coefficient in these limits are compared for pulsed and continuous-wave light sources.

OCIS codes: 000.2170, 020.3690, 120.3930, 300.3700, 300.6390.

1. Introduction

An incredible growth in use of the cavity ringdown technique has occurred during the past decade.[1–3] One of the much heralded merits of cavity ringdown spectroscopy (CRDS) is the sensitivity with which absorption coefficient measurements can be made.[3,4] In fact, in the shot-noise limit, the noise-equivalent absorption coefficient lies between 10^{-8} and 10^{-13} cm^{-1} Hz$^{-1/2}$ for realistic cavity and laser parameters. At the lower limit, this sensitivity corresponds to a number density of 10^{12} m^{-3} water molecules if the (101) $\leftarrow$ (000) band were probed and 10^{9} m^{-3} molecules of carbon dioxide using the (00011) $\leftarrow$ (00001) band. This sensitivity makes the technique attractive for measuring the residual gases in vacuum systems or the trace constituents of bulk gases. The associated precision hints at the possibility of a primary pressure standard based on absorption coefficient measurements. We have argued previously that the most sensitive and precise measurements can be made using a single-mode approach to CRDS.[5,6] In this paper we demonstrate an implementation of single-mode CRDS, using a pulsed laser system, with sensitivity near the shot-noise limit.

Figure 1 illustrates the concept of pulsed, single-mode CRDS.[5–7] Panels (a) and (b) show the power spectrum and the temporal shape, respectively, of a pulse of light incident on the cavity. Superimposed on the spectrum is the cavity's longitudinal-mode structure. The resonances of this progression, representing a single transverse series [i.e., fixed (m, n) indices], are separated by the free spectral range (FSR), which is equal to the speed of light c divided by twice the cavity length l (FSR is $c/2l$). For the high-reflectivity mirrors used in ringdown cavities ($R > 0.9999$, typically), a Lorentzian function provides an excellent approximation to the functional form of each peak, but for the high-finesse cavities typical of CRDS the widths are so narrow (from 10 kHz to 0.5 MHz) that individual modes appear as vertical lines on the abscissa of panel (a). Panel (c) shows the spectrum of the exiting flux, and panel (d) the corresponding time profile. The spectral profile is greatly altered because of the inherent frequency selectivity of a ringdown cavity. To do pulsed single-mode CRDS, the length of the cavity must be chosen so that its FSR is large compared with the spectrum of the incident field, as shown in panel (a). This choice allows a single cavity mode to be excited, which ensures that the decay signal will be a simple exponential, as shown in panel (d). Similarly, when a single mode is excited, transverse-mode beating cannot occur. Furthermore, because the ringdown cavity is excited with light spanning a narrow frequency interval, there is no need to deconvolute the decay signals spectrally. In contrast to single-mode CRDS, in conventional pulsed CRDS the incident spectrum is significantly larger than the cavity's

The authors are with the Chemical Science and Technology Laboratory, National Institute of Standards and Technology, 100 Bureau Drive, Gaithersburg, Maryland 20899-8364.

Received 23 November 1998; revised manuscript received 3 February 1999.

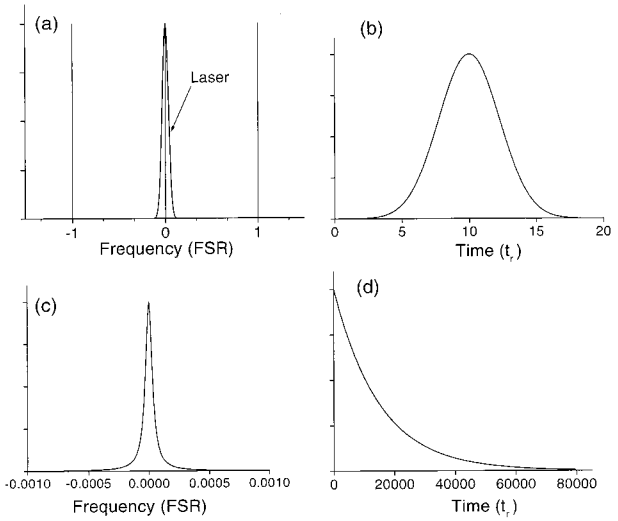

Fig. 1. Illustration of the concept of single-mode CRDS using realistic experimental parameters. Panels (a) and (b) show, respectively, the power spectrum of the incident light compared with the cavity mode spectrum, plotted in units of the free spectral range (FSR is $c/2l$) and the temporal profile of the incident light, plotted in units of the cavity round-trip time ($t_r = 2l/c$). Panel (c) shows the spectrum of the exiting radiation, and panel (d) shows the simple exponential decay signal expected as a result of exciting a single mode.

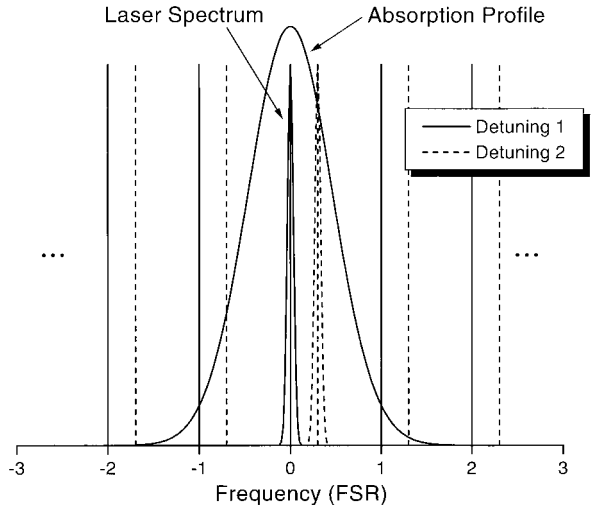

Fig. 2. Illustration of the measurement of the absorption coefficient as a continuous function of frequency using single-mode CRDS. Initially, the laser and the cavity resonance are at one frequency (solid curves). The ring-down time, and thereby the absorption coefficient, is measured. The laser frequency is then changed, and the cavity length is varied so the cavity resonances are shifted to follow the laser (dashed curves). The abscissa is in units of the cavity FSR.

FSR, and consequently light is coupled into several longitudinal—and usually transverse—modes.[5,7,8] This multimode excitation gives a ringdown signal that is a recurring series of pulses arising from longitudinal-mode beating and, when the incident light is not well mode matched into the cavity, transverse-mode beating. As light leaks from the cavity or is absorbed, this complicated signal slowly decays. Often, ringdown signals are electronically filtered to remove the faster beat notes from the slower decay. However, this decaying envelope can be a multiexponential function because the modes that are excited will have different absorptive losses, and different transverse modes can have differing empty-cavity losses. Extracting quantitative data from these ringdown signals therefore requires deconvolving the contributions of the excited modes. In addition to being cumbersome, this deconvolution compromises measurement sensitivity.[8–11]

As shown in Fig. 1 and discussed thus far, the cavity length has been fixed, which dictates that only the narrow frequency interval about the cavity resonance is transmitted. However, when measuring absorption spectra with single-mode CRDS, one wishes to measure the spectra as a continuous function of frequency. There is a solution to this conundrum: vary the cavity length. By tuning the center frequency of the incident light and concomitantly varying the cavity length to keep the cavity resonance tuned to the center frequency, as illustrated in Fig. 2, complete and continuous absorption spectra, requiring no deconvolution, can be measured with single-mode CRDS.

Using the single-mode approach offers important advantages over the conventional multimode, long-cavity implementation of CRDS. The most important of these is that, as already noted, the ringdown signal as a function of time is a single exponential. Specifically, for a transform-limited Gaussian pulse that is tuned onto a single cavity mode, the measured voltage is given by[5–7]

$$V(t;\omega) = \mathcal{E}_p f_{mn} \frac{\sqrt{2\pi}}{\sigma_\omega}\left[\frac{c(1-R)}{2l}\right]^2 \mathcal{R}G \exp\left[-\frac{t}{\tau(\omega)}\right] + V_{\mathrm{bl}} + \epsilon(t), \quad (1)$$

if we assume that the photodetection system faithfully replicates the exponential form of the ringdown signal. In Eq. (1) the first terms account for the quantity of light that gets into the ringdown cavity: $\mathcal{E}_p$ is the pulse energy incident on the cavity and f_{mn} is the fraction of the incident energy that couples into the transverse mode (m, n). The next two factors account for the spectral overlap between the incident field and the cavity mode, where the incident field has an $\exp(-1/2)$ power spectrum width of σ_ω (in dimensions of angular frequency ω) and the cavity is of length l with mirrors of reflectivity R. The detector responsivity $\mathcal{R}$ and transresistance gain G account for the conversion of the exiting optical power into a voltage. The next term in the product is the exponential decay in time t of the signal, with a time constant called the ringdown time $\tau(\omega)$. Any baseline signal is accounted for by V_{bl} and noise by $\epsilon(t)$.

The time constant of the decay, the ringdown time $\tau(\omega)$, depends on the mirror reflectivity and varies

across an absorption profile according to the function[6,7]

$$\tau(\omega) = \frac{l}{c[(1 - R) + \alpha(\omega)l]}, \tag{2}$$

where $\alpha(\omega)$ is the sample absorption coefficient. Rearranging Eq. (2) yields the following simple expression for $\alpha(\omega)$:

$$\alpha(\omega) = \frac{\tau_{\text{empty}} - \tau(\omega)}{c\tau_{\text{empty}}\tau(\omega)}. \tag{3}$$

Thus measuring the absorption coefficient simply involves determining two time constants [$\tau_{\text{empty}} \equiv$ ringdown time for an empty cavity or at a frequency where $\alpha(\omega) \approx 0$]. It is worthwhile to note that extracting the absorption coefficient does not depend on the actual length of the ringdown cavity, a unique and simplifying feature of CRDS.

The absorption coefficient itself is related to the number density of the absorbing species n, the line strength S, and the integral-normalized line-shape function $f(\omega)$ through the relationship[12]

$$\alpha(\omega) = 2\pi cnSf(\omega). \tag{4}$$

Accordingly, if partial pressure and temperature are known, n can be calculated and the product $Sf(\omega)$ can be determined from Eq. (3). Similarly, if S and $f(\omega)$ are known, the number density can be extracted.

In this paper we discuss an implementation of single-mode CRDS. First, the experimental apparatus is described. The measurement of this system's noise-equivalent absorption coefficient and a rovibronic line strength of molecular oxygen are presented to illustrate the power of the single-mode approach to CRDS. The effects of normally distributed noise on the relative standard deviation in the ringdown time and absorption coefficient are discussed. Finally, the detection limits in pulsed and cw single-mode CRDS experiments are compared, and the potential use of single-mode CRDS for standards measurements is discussed.

2. Experiment

A frequency-stabilized laser system and a length-stabilized ringdown cavity are required to implement successfully a single-mode cavity ringdown experiment. The following paragraphs describe the apparatus[13] and data reduction process used here to illustrate single-mode CRDS.

A. Ringdown Cavity

Although a ringdown cavity has inherent frequency selectivity, variations in the cavity length will cause the transmitted frequency to vary. The equation $\delta l = (\delta\omega/\omega)l$ helps quantify the magnitude of the stability required. At optical frequencies, to achieve ~1-MHz frequency stability, the cavity length variations must be <0.25 nm. For these experiments, stabilization was achieved by constructing a chamber from a nickel–iron austenitic alloy, chosen for its comparatively low coefficient of thermal expansion ($\leq 10^{-6}$ K^{-1}), and housing the ringdown assembly in a temperature-regulated enclosure. A platinum resistance thermometer was embedded in the chamber's body to monitor the temperature. The diurnal temperature stability was ±10 mK, and the short-term (~1-h) stability was better than ±2 mK. The uncertainty in the temperature measurement was estimated to ~10 mK. A diaphragm-backed drag pump evacuated the *O*-ring sealed cavity, and a capacitance diaphragm gauge was used to measure the chamber pressure. The chamber pumped down to <100 mPa; when the valve connecting the chamber to the pump was closed, the leak rate was ~3 Pa h^{-1}. The cavity was filled to ~0.2 kPa for the spectra shown below. This pressure measurement had an uncertainty of ≤1%. Oxygen with a stated purity of 99.999% was used without further purification, and the sample was assumed to be composed of isotopes in the naturally occurring abundances.

A pair of 20-cm radius-of-curvature dielectric mirrors ~10.5 cm apart formed the ringdown cavity. Total empty cavity losses varied between 25×10^{-6} and 45×10^{-6} per pass depending on the cleanliness of the mirrors and cavity alignment. One mirror was attached to a tubular piezoelectric element, which permitted scanning of the ringdown cavity length and hence the cavity resonant frequency. This cavity length and mirror curvature combination corresponds closely to the degenerate condition in which the longitudinal- and transverse-mode spacings are 1.5 GHz and 500 MHz, respectively. This geometry was chosen so that the transverse-mode spacing greatly exceeded the width of the field spectrum of the incident laser light.

B. Light Source

Light for these measurements was generated with an injection-seeded, pulsed optical parameter oscillator (OPO) similar in design to that described by Alford and co-workers.[14,15] The oscillator was a singly resonant, three flat-mirror ring arranged to form a right, isosceles triangle. The geometric length of the ring was nominally 12 cm. A 1-cm-long potassium titanyl phosphate crystal cut for type II critical phase matching served as the optical parametric-generating medium. The frequency-doubled, spatially filtered output of a 10-Hz, injection-seeded Nd^{3+}:YAG laser pumped the OPO crystal. The ~760-nm output of a cw, external-cavity diode laser seeded the OPO signal wave. The oscillator ring was dither locked to this seed laser, and firing of the pump laser was synchronized to the dither so as to minimize frequency jitter. The seed laser, in turn, was frequency stabilized against a transfer cavity. This 30-cm-long transfer cavity,[16,17] to which both the OPO and Nd^{3+}:YAG's seed lasers can be locked, was itself locked to a commercial He–Ne laser that was frequency stabilized by intensity balancing the polarized light of adjacent longitudinal modes. This He–Ne laser provided the absolute frequency stability of the system, and the drift in the central fre-

quency of this laser was measured, by monitoring the heterodyne signal generated by beating against an iodine-stabilized He–Ne laser, to be ~1 MHz per day. The error signals for locking the transfer cavity and the seed lasers were produced using the standard dither-lock scheme. Before being directed to the transfer cavity, the seed laser was double passed through an acousto-optic modulator. The modulator and beam were aligned in a way that eliminated deflection of the beam after the second pass.[18] Furthermore, the double pass gave a net frequency shift of up to 250 MHz, which allowed tuning of the seeded laser from one transverse mode of the transfer cavity to the next. The resulting frequency stability was estimated from the fluctuations in the error signals to be better than 3 MHz. In seeded operation and when pumped with a fluence of ~2 J cm^{-2}, the OPO generated ~1 mJ of signal light in an ~4.5-ns-long pulse. The power spectrum was measured by holding the OPO frequency fixed and scanning the ringdown cavity through an isolated cavity resonance. The power spectrum was well characterized by a Gaussian function with a full width at half-maximum (FWHM) spectral bandwidth of ~115 MHz. The M^2 statistic,[19] a comparison of the beam to a diffraction-limited beam, was 3.4 and 4.7 in the horizontal and vertical directions, respectively.

Several measures maximized coupling into the lowest-order transverse-electromagnetic mode (TEM_{00}). The OPO beam was spatially filtered using a lens and a ruby pinhole, and the waist at the pinhole was imaged[20] into the ringdown cavity with a second lens. The mirrors that directed the light to the cavity were mounted on a translation stage, which permitted control of the position of the waist created by the second lens. By fixing the OPO frequency and scanning the cavity length over a FSR of the cavity, different transverse modes could be observed with a charge-coupled device camera and photodiode. This procedure made it possible to adjust the alignment so as to maximize coupling into the TEM_{00}. More than three quarters of the transmitted light was in the TEM_{00} mode, and no mode with a transverse-mode index sum $(m + n)$ greater than 2 was appreciably excited.

C. Data Acquisition and Reduction

A commercial Si-p-i-n photodiode and amplifier package with a 125-MHz bandwidth was used to monitor the ringdown signals. The output was terminated into 50 Ω at the input of an analog-to-digital converter that sampled the signal at a rate of $\leq 10^8$ Hz. The digitized ringdown signals were transferred to a computer and processed on a shot-by-shot basis.

Decay time constants were determined from weighted least-squares regressions to individual ringdown curves.[21] The average value of the baseline signal that immediately preceded each exponential decay was determined and subtracted from the ringdown signal. After taking the natural logarithm of the baseline-corrected signal to linearize the signal, the ringdown time constant as well as the initial signal level was extracted from the best-fit slope and intercept, respectively. A best estimate of the variance was used to weight each point along the ringdown curve.[21]

The variance of the ith sample along the single exponential decays observed in the experiments reported here can be grouped into two components: shot noise on the exiting photon flux and technical noise in the detection system. The shot noise is a function of the signal level V_i (units of volts), photon energy $\hbar\omega$, digitization time interval Δt, the detector responsivity $\mathcal{R}$ (units of amperes per watt), and transresistance gain G (units of volts per ampere). There are two contributors to the technical-noise variance σ_{tech}^2: the detection system variance and a digitizer variance. The first of these, the detection system variance σ_{ds}^2, accounts for electrical noise in the photodiode and amplifier, cabling, and digitizer circuit. The other, the digitizing variance, arises from the finite vertical voltage resolution of the digitizer and is a function of the full-scale voltage V_{fs} and the number of bins N. If the noise sources are large compared to an individual bin $[(\sigma_{\text{shot noise}}^2 + \sigma_{\text{ds}}^2)^{1/2} > V_{\text{fs}}/N]$, the probability that a sample will land at a particular location across the bin should, on average, be constant. The probability distribution is therefore rectangular, and the variance can be computed and added to the others. Summing these three, the shot noise, the detection system noise, and the digitization variances, gives the total variance in the ith point σ_i^2 in the ringdown curve. Before transformation from linear to logarithmic coordinates, for σ_i^2 this summation gives

$$\sigma_i^2 = \frac{\hbar\omega\mathcal{R}GV_i}{\Delta t} + \sigma_{\text{ds}}^2 + \frac{1}{3}\left(\frac{V_{\text{fs}}}{2N}\right)^2. \tag{5}$$

Operationally, the shot noise was calculated using parameters for the detector that was used in these experiments, and the measured variance in the baseline preceding the ringdown signal was taken as a measure of the technical-noise variance throughout the ringdown curve.

Inspection of Eq. (5) reveals that, if at the beginning of a ringdown curve technical noise dominates the variance, then it will do so throughout the ringdown curve, and even if the shot-noise term dominates at first, the technical noise will eventually surpass the shot-noise term. This trend is expected because the technical noise is unchanged throughout a ringdown curve whereas the shot noise decreases as the signal decreases. For CRDS, a shot-noise-limited ringdown curve can be defined as a decay trace for which the shot-noise term constitutes the major portion of the combined variance over some significant fraction (e.g., three time constants) of the overall ringdown curve.

3. Results

In this section we discuss data gathered using the pulsed single-mode CRDS apparatus described above. First, individual ringdown traces and the as-

sociated statistics are considered. Then spectra of an individual rovibronic line of the molecular oxygen *A* band are shown for neat, rarefied oxygen and for oxygen mixed with molecular nitrogen at pressures at which the line profile broadens. The statistics associated with these line-shape measurements are also discussed.

A. Individual Ringdown Curves

The precision with which the ringdown time constant is measured ultimately determines the precision with which a line strength or number density can be measured. As discussed above, the uncertainty in the ringdown time will be minimized when shot noise dominates the noise along most of the ringdown curve. In this case, the relative standard deviation in the ringdown time will simply be the reciprocal of the square root of the number of detected photons[4,6,7] or,

$$\frac{\sigma_\tau}{\tau(\omega)} = \left[\frac{2l}{c(1-R)}\right]\left[\frac{\sigma_\omega \hbar\omega}{\sqrt{2\pi}\,\mathscr{E}_p f_{mn}\tau(\omega)}\right]^{1/2}. \qquad (6)$$

Experimentally, this limit is asymptotically approached when the sampling rate is fast compared with the ringdown time and the technical noise is brought below the shot noise for some significant fraction of the ringdown time. The residuals of an exponential fit from a near-shot-noise-limited ringdown curve will be randomly distributed within a band that looks like a funnel, with the largest residuals at early times, where the signal is largest. For later times, the residuals will then be confined to a constant band determined by the technical noise. If, on the other hand, technical noise dominates throughout a ringdown curve and each point is statistically independent,[22] the relative standard deviation in the ringdown time is

$$\frac{\sigma_\tau}{\tau(\omega)} = \frac{2\sigma_{\text{tech}}}{V(t=0;\,\omega)}\left[\frac{2\Delta t}{\tau(\omega)}\right]^{1/2}. \qquad (7)$$

In the technical-noise limit, the residuals to an exponential fit will be distributed within a constant band with time.

Figure 3 displays a typical ringdown curve. The signal exhibits simple exponential behavior over five time constants. The value of reduced $\chi^2 = 1.08$ confirms that Eq. (1) models the data well and that the data have been correctly weighted.[21] The relative standard deviation in the ringdown time σ_τ/τ was extracted along with the fit parameters and equals 3×10^{-4}. Plotted beneath the signal are the fit residuals. Within the signal-to-noise limits of this data, these residuals show no systematic effects such as mode beating and are constant, indicating that technical noise dominates. The striation in the residuals at long times is an artifact of the digitization process.

Examining the statistics associated with many independent measurements of the ringdown time can provide additional information about the measurement precision. When the shot-to-shot variations in the ringdown time result from statistical rather than systematic effects, the fractional uncertainty determined from fitting an individual curve (σ_τ/τ) should be the same as the relative standard deviation from the ensemble of independent measurements ($\sigma_{\tau,\text{ens}}/\bar{\tau}$), where $\sigma_{\tau,\text{ens}}$ and $\bar{\tau}$ are the standard deviation and mean value, respectively, of the ensemble of ringdown times.[21] In addition, in the ideal case the measurements should be normally distributed about the mean. In practice this condition is not always met, and ensemble-based uncertainties in ringdown times often are found to be greater than those determined from fits to individual traces, thereby diminishing the sensitivity of the measurement. Such nonideal behavior can be linked to factors including low-frequency electronic noise or drift, inadequate determination of the baseline, and multimode excitation of the ringdown cavity.

To demonstrate the equivalence of the single-shot statistics and the ensemble statistics, Fig. 4 exhibits cumulative probability distributions (CPD's).[23,24] The CPD for ringdown times extracted from fitting a set of 500 individual ringdown curves is shown in Fig. 4 by the open circles. From these independent mea-

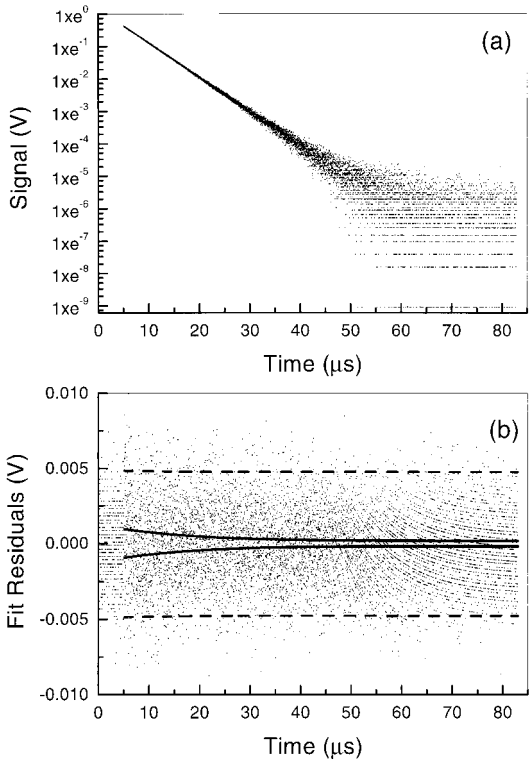

Fig. 3. Panel (a) shows a typical ring-down curve after the baseline has been subtracted. Note that the data span nine time constants. The best-fit value of the ring-down time is 9.502 μs, with a relative standard deviation σ_τ/τ of 3×10^{-4}. Panel (b) shows the residuals to the fit. The solid curves are twice the standard deviation for the shot noise at the fluence of this trace, and the dashed curve is twice the standard deviation for the technical noise measured in the baseline preceeding the ring-down signal.

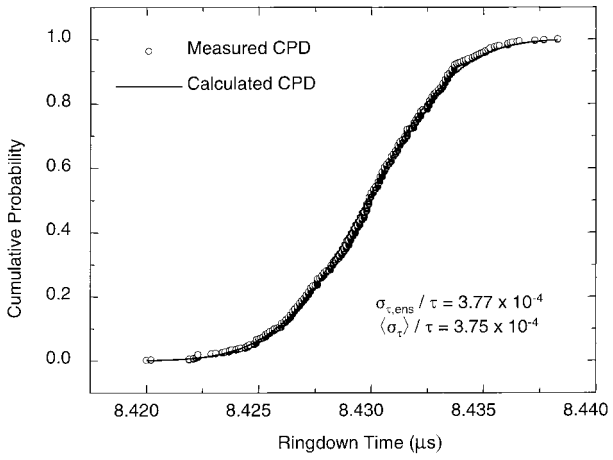

Fig. 4. Cumulative probability distributions (i.e., the fraction of an ensemble of independent measurements with a value equal to or less than a given value of τ as a function of τ) for the measured (open circles) and a calculated distribution (solid curve). The measured distribution is based on 500 ring-down measurements. The calculated distribution is based on the mean standard deviation extracted from individual fits to ring-down curves $\langle\sigma_\tau\rangle$ and the mean ring-down time $\bar{\tau}$.

surements, $\bar{\tau}$ and $\sigma_{\tau,ens}$ were computed. For each of the individual ringdown curves, the standard deviation in the fit-determined ringdown time σ_τ was also calculated,[21] and from these the mean fit-based standard deviation in the ringdown time $\langle\sigma_\tau\rangle$ can easily be determined. The CPD for a normal distribution can then be calculated using $\langle\sigma_\tau\rangle$ and $\bar{\tau}$. This calculated distribution is superimposed on the measured CPD in Fig. 4. Visual inspection shows that the two distributions are in good agreement. The extent of agreement can be quantified with the Kolmogorov–Smirnov statistic.[23,24] This statistic tests the hypothesis that two CPD's represent the same parent distribution. For the data and the normal CPD shown in Fig. 4, the Kolmogorov–Smirnov statistic is 0.004, indicating a far less than 1% probability that the measured and calculated distributions are different.[23,24] Furthermore, this observation demonstrates that shot-to-shot variations in this experiment are not driven by unexplained fluctuations in the properties of the incident light or the ringdown cavity.

Measurement of the ensemble statistics allows calculation of the noise-equivalent absorption (NEA) coefficient. For data collection at a rate of f_{rep}, the NEA is[4,6]

$$\mathrm{NEA} = (2/f_{rep})^{1/2} \frac{\sigma_{\tau,ens}}{c\bar{\tau}^2}. \tag{8}$$

Equation (8) shows that decreasing $\sigma_{\tau,ens}$ or increasing the repetition rate or ringdown time decreases the NEA. For the statistics presented above, the NEA is 5×10^{-10} cm^{-1} Hz$^{-1/2}$, indicating that an absorption coefficient of 5×10^{-10} cm^{-1} could be distinguished from empty cavity losses during a 1-s measurement interval, with 68% or one sigma certainty, provided that the repetition rate is large enough to determine adequately the relative standard deviation.

With the aid of Eq. (7) and an independent measurement of the various noise levels in the experiment, it should be possible to predict the relative standard deviation of τ in these measurements. The noise in the photodiode and amplifier circuit over the bandwidth of the digitizer is ~1.5 mV. On the 1-V scale typically used in these experiments, the digitizer has ~1 mV of noise. The bin size is 0.24 mV. When added in quadrature, these numbers yield a σ_{tech} of ~2 mV. For a ringdown signal sampled at 10^8 Hz and having an initial level of 0.7 V, this standard deviation, in turn, predicts a relative standard deviation in the ringdown time of 2.7×10^{-4}. This result is in good agreement with the measured value of 3×10^{-4} reported above. Furthermore, this agreement and the CPD comparison indicate that the highest sensitivity possible, given the current noise levels, has been reached. Ultimate sensitivity comes, however, when both the single-shot statistics and the CPD are at the shot-noise limit. Under typical operating conditions, from 4×10^8 to 1×10^9 photons are detected in each ringdown curve. Therefore the relative standard deviation in the ringdown time would be between 5×10^{-5} and 3.2×10^{-5}, six to ten times smaller than the measured value reported above. Decreasing the noise in the photodiode and amplifier package, perhaps by using a detection system with the minimum bandwidth necessary to maintain the fidelity of the signal, and decreasing the noise in the analog-to-digital conversion process, perhaps by using a heterodyne detection scheme,[25,26] should make ensemble-based measurements at the shot-noise limit possible.

B. Spectra Measured with Pulsed Single-Mode Cavity Ringdown Spectroscopy

Because a line shape will vary with total pressure and because it can be difficult to know the exact frequency detuning, one might anticipate that, from a practical stance, the product of the number density and the line strength nS could best be measured by recording an entire spectrum. Rewriting Eq. (2) as

$$\frac{1}{\tau(\omega)c} = \frac{1}{\tau_{empty}c} + nSf(\omega) \tag{9}$$

shows that the product nS can be extracted from a linear regression of the measured losses as a function of $f(\omega)$ if the line-shape function is known. Again, note that only ringdown times must be measured to determine the nS product. The uncertainties associated with these fit parameters can again be calculated, although they cannot be expressed in a simple, closed form. For a reasonable ratio of mirror to absorptive losses (say, between 1 and 100) and adequate sampling of the absorption profile and baseline (say, ten or more points across the FWHM and a total scan of four or more FWHM with P total points), numerical simulations show that the relative standard devia-

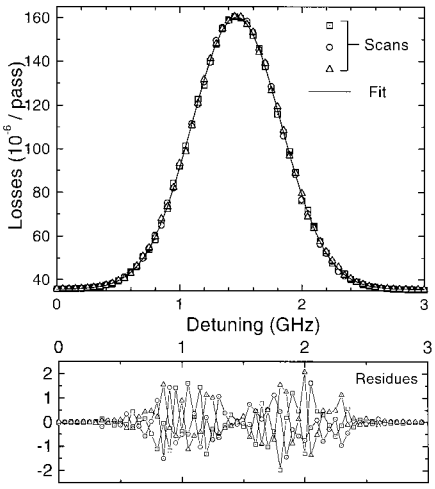

Fig. 5. Three spectra of the $^{P}Q(9)$ line of the A band of $^{16}O_2$ and a fit of a Doppler profile to the data. The best-fit parameters were peak losses of 124.9×10^{-6} per pass, a FWHM of 857.8 MHz, and empty cavity losses of 35.6×10^{-6} per pass. The pressure was 199 Pa.

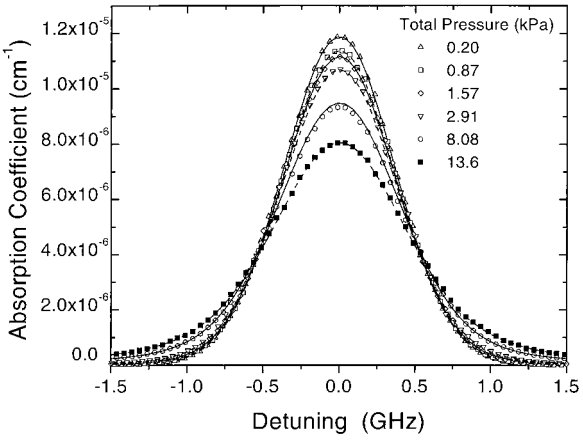

Fig. 6. Pressure-broadened spectra of the $^{P}Q(9)$ line of the A band of $^{16}O_2$. The partial pressure of oxygen was ~0.2 kPa in each scan. Superimposed on each spectrum is a fit using the Galatry line-shape function and effective line-shape parameters, that is, the mole-fraction-weighed sum of the O_2–N_2 and O_2–O_2 parameters.

tion in the number density line strength product σ_{nS}/nS scales as

$$\frac{\sigma_{nS}}{nS} \sim \frac{\sigma_\tau}{\tau} P^{-1/2}. \tag{10}$$

Spectra of the $^{P}Q(9)$ transition of the A band[27,28] of $^{16}O_2$ at 13093.64 cm^{-1} were measured to evaluate the precision to which single-mode CRDS could measure an integrated line strength. The center frequency of the OPO was varied in 50-MHz increments, and the cavity length was varied to maintain resonance with the OPO. At each frequency, ten individual ringdown time constants were extracted from ten ringdown curves, and the average was calculated.

Figure 5 displays three consecutive measurements of the $^{P}Q(9)$ line at a pressure of 199 Pa. Given the level of technical noise seen in Subsection 3.A, it could be anticipated that the relative scatter in the data would be $<10^{-3}$ at each detuning. Clearly, however, the scatter between the independent measurements exceeds this bound. The increased scatter arises because there is an uncertainty of ~5 MHz between the cavity resonance frequency and the OPO frequency at each detuning. This uncertainty results in a larger than expected variation in the cavity losses at each detuning from scan to scan. Active locking of the ringdown cavity to the reference He–Ne laser or to the seed of the OPO, perhaps by a heterodyne beat between the seed and the ringdown signal,[29] would reduce this frequency error.

Also shown in Fig. 5 is a fit of a Doppler profile to the data, weighted by the reciprocal of the variance of the measurements at that detuning. Eighteen similar spectra were recorded over a period of a month and individually fit, again using a Doppler line-shape and published line-shape parameters. The line strength was determined from a weighted linear regression of Eq. (8). From these spectra, the line strength for this transition was determined to be 7.44×10^{-24} cm^{-1} (molecule cm^{-2}) with a standard deviation of 1%. The absolute value for the line strength is 0.6% lower than the commonly used value.[28] The relative standard deviation in the multiple-scans number reflects both the uncertainty in the frequency axis already noted and the instabilities and nonlinearities in digitization.

C. Pressure-Broadened Spectra Measured with Pulsed Single-Mode Cavity Ringdown Spectroscopy

Conventional CRDS has already been used to measure line shapes.[11,30–32] To illustrate use of pulsed single-mode CRDS to measure line shapes, the change in the line shape for the $^{P}Q(9)$ line of the A-band transition of molecular oxygen is presented in Fig. 6. Here the line shape is shown for a neat sample of oxygen at ~0.2 kPa at 295.6 K, at which pressure the line is essentially Doppler broadened. With this fixed oxygen pressure, varying amounts of molecular nitrogen were added. The expected increase in linewidth is observed with increasing nitrogen pressure. The line strength can be extracted from these spectra, using published values for the line-shape parameters and a Galatry line-shape function.[28] Because there are two collision partners, it was assumed that the effective narrowing and broadening parameters were given by the mole-fraction-weighted sum of the respective narrowing and broadening parameters. The fits at each pressure are superimposed on the measured data. The mean line strength determined from these data was 7.31×10^{-24} cm^{-1} (molecule $cm^{-2})^{-1}$, a value 1.1% less than that reported above and approximately 2% below the commonly used value.[28] The spectra comprising this data set were obtained over the course of two weeks, and the standard deviation in the extracted line strength was equal to 0.28% of the mean value.

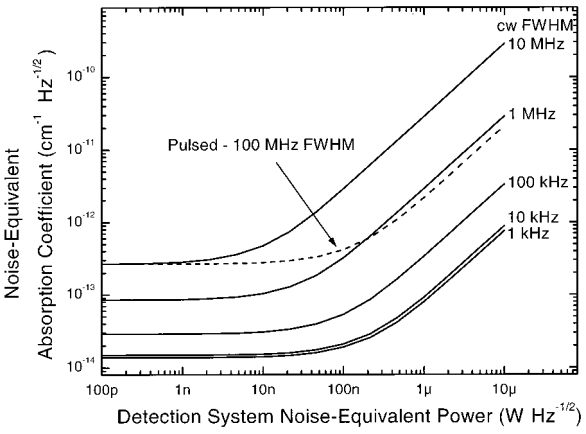

Fig. 7. NEA coefficient as a function of detection system NEP for cw and pulsed excitation of a 0.5-m-long ring-down cavity constructed with mirrors of $R = 0.999965$. In all cases, 10 mW was assumed to be incident on the cavity, although the cw linewidth of the incident light varied as noted in the figure. See Section 4 for further details.

This number is considerably smaller than the standard deviation reported above, largely because a digitizer with better precision, linearity, and long-term stability was used for these measurements. Also the difference between the two extracted line strengths is attributed largely to differences in the digitizers used for the two sets of measurements, and consequently the extracted line strength of 7.31×10^{-24} cm^{-1} (molecule cm^{-2})$^{-1}$ is believed to be the most accurate of the two measured values reported in this paper.

4. Discussion

A. Pulsed and Continuous-Wave Single-Mode Cavity Ringdown Spectroscopy

As noted in Section 1, one merit of CRDS is the sensitivity that the technique offers. In Fig. 7, the NEA coefficient is plotted as a function of detector noise-equivalent power (NEP) of the detection system. Two families of curves are plotted. The dashed curve represents the NEA for a pulsed laser with a power spectrum of 100 MHz FWHM, similar to the laser used in these experiments. The solid curves are the same quantity for excitation of a ringdown cavity by a cw source, which would be pulsed by deflecting the light away from the cavity, perhaps using an acousto-optic modulator, so that ringdown measurements could be made.[33–35] For both light sources, the calculations assumed a 50-cm-long cavity, 10 mW of incident power, mirror losses of 35×10^{-6}, and that data were acquired at the maximum possible repetition rate; to wit, 10 Hz for the pulsed laser and 2.1 kHz for the cw system, which corresponds to a ten time constant delay between consecutive measurements in the latter case.

All the curves share a common general form. For low values of NEP, the NEA is constant, then begins increasing as NEP increases, eventually increasing linearly with NEP. These features are easily understood. At the low NEP values, the contribution of technical noise to the relative standard deviation in τ is negligible; only shot noise, which does not vary, contributes. Accordingly, NEA is unaffected and constant. At some point, depending on the initial value of the signal, which in turn depends on the ratio of the laser-to-cavity linewidths, technical noise begins to contribute to the relative standard deviation in τ, and NEA begins to increase. When only technical noise contributes to the relative standard deviation in τ, NEA continues to increase and does so linearly in the NEP, as Eqs. (3) and (7) predict.

Comparison of the relative values of the pulsed and cw laser NEA values is another point to be observed from Fig. 7. For reference, it should be noted that a typical commercial Si-p-i-n detector and amplifier will have a NEP between 10 nW Hz$^{-1/2}$ and 0.5 μW Hz$^{-1/2}$, and an infrared wavelength-sensitive detector of comparable bandwidth will generally have a larger NEP. In the shot-noise limit, the NEA is smaller for cw excitation than pulsed excitation for all the cases considered here, except the 10-MHz cw linewidth case, corresponding, for example, to a distributed-feedback diode laser. As the cw laser's spectrum narrows, more light is coupled into the cavity and NEA decreases until essentially all the incident photons can couple into the cavity.

The situation in the technical-noise limit is somewhat more complicated, however. Here pulsed measurements hold an advantage over cw measurements because, usually, the initial signal size is greater in the pulsed case, and the relative standard deviation in the ringdown time is inversely proportional to the initial signal size [see Eq. (7)]. However, when the FWHM of a cw source is <1 MHz, the increased repetition rate of the cw measurement decreases the NEA compared with the pulsed case, despite the fact that the relative standard deviation in the ringdown time (σ_τ/τ) is larger than in the pulsed measurement [see Eq. (8)]. When the cw laser linewidth is narrower than the cavity resonance, however, the initial intensity becomes larger in the cw measurement than in the pulsed measurement, which reduces the relative standard deviation in the ringdown time [compare with Eq. (7)]. The combined advantages of a small relative standard deviation and the comparatively high repetition rate [see Eq. (8)] thereby give a NEA approximately 100 times smaller in the cw case than in the pulsed case in this limit.

Many factors could complicate the simplified picture presented here; most notably, an exact comparison requires comparing specific lasers for a specific experiment. Furthermore, a laboratory implementation can be quite different from a conceptualization. For example, mode matching might be imperfect, thereby decreasing the flux transmitted through the cavity and increasing the NEA. In fact, we found it difficult to achieve field coupling coefficients greater than approximately 10%. In addition, at the highest fluences, detectors would be expected to saturate, making it impossible to take advantage of the added flux. Nevertheless, these observations point out

general trends and advantageous measurement domains.

B. Pressure Measurements with Single-Mode Cavity Ringdown Spectroscopy

It is interesting to consider the use of CRDS as a pressure standard.[13] Existing pressure standards at the National Institute of Standards and Technology have fractional uncertainties of 10^{-2} to 10^{-3} between 1 μPa and 10 Pa and 10^{-3} to 10^{-5} between 10 Pa and 5 kPa. At the shot-noise limit, the uncertainties associated with a ringdown measurement are competitive with the uncertainties of these present standards. For such a standard to be realized, the line strength must be known with the requisite precision and accuracy. For example, the quadrupole lines of molecular hydrogen[36,37] have integrated line strengths of the order of 10^{-29} to 10^{-26} cm^{-1} (molecules $cm^{-2})^{-1}$ and could, perhaps, be calculated from first principles with the needed accuracy. These lines could be used to measure pressures between 1 kPa and 1 MPa. Alternatively, the line strength could be measured at a point where the number density is well known. An example of such a molecule would be water because the vapor pressure at its triple point[38] has a fractional uncertainty $<2 \times 10^{-5}$. The line strength of one or more rovibronic transitions of water could be measured at the triple point. This measurement would yield a line strength that could be used to measure number densities at other temperatures and pressures.

An absolute measurement standard demands not only precision, which has been the focus of the research presented here, but also accuracy. Systematic errors arising from inaccuracy in the measurement of the time and frequency shifts, nonlinearity in signal detection, or any unexpected contribution to the signal can contribute to measurement inaccuracy. Further experiments and improvements in the measurement technique will be required to make a reliable assessment of the system errors. However, based on this research to date, the linearity of the photoreceiver and electronics are already known to be important factors that limit the accuracy to which the quantity nS can be determined.

5. Conclusion

We have discussed the use of pulsed lasers to carry out single-mode cavity ring-down spectroscopy and the effects of normally distributed noise on the measurement uncertainty. A relative standard deviation of $\sim 3 \times 10^{-4}$ in the ringdown time was measured on individual ringdown curves and on a set of several hundred independent measurements. This number is less than a decade away from the shot-noise limit at current fluences. Line strengths were measured for a rovibronic transition of molecular oxygen both in the Doppler limit and in the pressure-broadened case. The relative standard deviation in the measured quantity was found to be $<0.3\%$ and agreed well with previous measurements of the same transition. Comparison of a NEA coefficient for pulsed and cw single-mode CRDS measurements showed that, for many typical measurement configurations, pulsed measurements can give sensitivities comparable with cw-based measurements.

We thank D. F. Plusquellic for his many helpful suggestions on the design and operation of the optical parametric oscillator and transfer cavity and G. T. Fraser, K. K. Lehmann, G. J. Rosasco, and D. C. Robie for carefully reading the draft manuscript.

References and Notes

1. O. E. De Lange, "Losses suffered by coherent light redirected and refocussed many times in an enclosed medium," Bell Syst. Tech. J. **44,** 283–302 (1965).
2. W. M. Hughes, N. T. Olson, and R. Hunter, "Experiments on 558-nm argon oxide laser system," Appl. Phys. Lett. **28,** 81–83 (1976).
3. A. O'Keefe and D. A. G. Deacon, "Cavity ring-down optical spectrometer for absorption measurements using pulsed laser sources," Rev. Sci. Instrum. **59,** 2544–2551 (1988).
4. D. Romanini and K. K. Lehmann, "Ring-down cavity absorption spectroscopy of the very weak HCN overtone band with six, seven, and eight stretching quanta," J. Chem. Phys. **99,** 6287–6301 (1993).
5. J. T. Hodges, J. P. Looney, and R. D. van Zee, "Response of a ring-down cavity to an arbitrary excitation," J. Chem. Phys. **105,** 10,278–10,288 (1996).
6. J. P. Looney, J. T. Hodges, and R. D. van Zee, "Quantitative absorption measurements using cavity-ringdown spectroscopy with pulsed lasers," in *Cavity-Ringdown Spectroscopy: An Ultratrace-Absorption Measurement Technique*, K. A. Busch and M. A. Busch, eds. (Oxford U. Press, Oxford, UK, 1998), Chap. 7.
7. K. K. Lehmann and D. Romanini, "The superposition principle and cavity ring-down spectroscopy," J. Chem. Phys. **105,** 10,263–10,277 (1996).
8. P. Zalicki and R. N. Zare, "Cavity ring-down spectroscopy for quantitative absorption measurements," J. Chem. Phys. **102,** 2708–2717 (1995).
9. J. T. Hodges, J. P. Looney, and R. D. van Zee, "Laser bandwidth effects in quantitative cavity ring-down spectroscopy," Appl. Opt. **35,** 4112–4116 (1996).
10. R. T. Jongma, M. G. H. Boogaarts, I. Holleman, and G. Meijer, "Trace gas detection with cavity ring down spectroscopy," Rev. Sci. Instrum. **66,** 2821–2827 (1995).
11. D. L. Huestis, R. A. Copeland, K. Knutsen, T. G. Slanger, R. T. Jongma, M. G. H. Boogaarts, and G. Meijer, "Branch intensities and oscillator strengths for the Herzberg absorption systems of oxygen," Can. J. Phys. **72,** 1109–1121 (1994).
12. L. A. Pugh and K. N. Rao, "Intensities from infrared spectra," in *Modern Spectroscopy*, K. N. Rao, ed. (Academic, New York, 1976), Vol. 1, pp. 165–177.
13. R. D. van Zee, J. P. Looney, and J. T. Hodges, "Measuring pressure with cavity ring-down spectroscopy," in *Advanced Sensors and Monitors for Process Industries and the Environment*, W. A. de Groot, ed., Proc. SPIE **3535,** 46–55 (1999).
14. W. J. Alford, T. D. Raymond, and A. V. Smith, "Characterization of a ring optical parametric oscillator," in *Advanced Solid-State Lasers*, T. Y. Fan and B. Chai, eds. Vol. 20, of OSA Proceedings Series (Optical Society of America, Washington, D. C., 1994), pp. 476–479.
15. A. V. Smith, W. J. Alford, T. D. Raymond, and M. S. Bowers, "Comparison of a numerical model with measured performance of a seeded, nanosecond KTP optical parametric oscillator," J. Opt. Soc. Am. B **12,** 2253–2267 (1995).
16. E. Riedle, S. H. Ashworth, J. T. Farrell, Jr., and D. J. Nesbitt,

"Stabilization and precise calibration of a continuous-wave difference frequency spectrometer by use of a simple transfer cavity," Rev. Sci. Instrum. **65,** 42–48 (1994).
17. D. F. Plusquellic, O. Votava, and D. J. Nesbitt, "Absolute frequency stabilization of an injection-seeded optical parametric oscillator," Appl. Opt. **35,** 1464–1472 (1996).
18. J. L. Hall, "Laser stabilization lectures," Fall Semester 1985, University of Colorado, Boulder, Colo.
19. A. E. Siegman, "New developments in laser resonators," in *Optical Resonators*, D. A. Holmes, ed., Proc. SPIE **1224,** 4–14 (1990).
20. H. Kogelnik and T. Li, "Laser beams and resonators," Proc. IEEE **54,** 1312–1329 (1966).
21. P. R. Bevington, *Data Reduction and Error Analysis for the Physical Sciences* (McGraw-Hill, New York, 1969), Chaps. 6, 9, and 10.
22. The data along a ring-down curve are not, strictly speaking, statistically independent because either the detector electronics or digitizer impose a bandwidth filter on the signal. K. K. Lehmann has derived formulas for fitting ring-down signals in which the data are correlated, and he will present these algorithms in a forthcoming publication.
23. R. von Mises, *Mathematical Theory of Probability and Statistics* (Academic, New York, 1964), Chaps. IX(C) and IX(E).
24. W. A. Press, B. P. Flannery, S. A. Teukolsky, and W. T. Vetterling, *Numerical Recipes* (Cambridge U. Press, Cambridge, UK, 1989), Chap. 13.
25. M. D. Levenson and G. L. Eesley, "Polarization selective optical heterodyne detection for dramatically improved sensitivity in laser spectroscopy," Appl. Phys. **19,** 1–17 (1979).
26. M. D. Levenson, B. A. Paldus, T. G. Spence, C. C. Harb, J. S. Harris, Jr., and R. N. Zare, "Optical heterodyne detection in cavity ring-down spectroscopy," Chem. Phys. Lett. **290,** 335–340 (1998).
27. H. D. Babcock and L. Herzberg, "Fine structure of the red system of atmospheric oxygen band," Astrophys. J. **108,** 167–190 (1948).
28. K. J. Ritter and T. D. Wilkerson, "High-resolution spectroscopy of the oxygen A-band," J. Mol. Spectrosc. **121,** 1–19 (1987).
29. D. C. Hovde, J. H. Timmermans, G. Scoles, and K. K. Lehmann, "High power, injection seeded optical parametric oscillator," Opt. Commun. **86,** 294–300 (1991).
30. D. Romanini and K. K. Lehmann, "Line-mixing in the $106 \leftarrow 000$ overtone transition of HCN," J. Chem. Phys. **105,** 81–88 (1996).
31. R. T. Jongma, M. G. H. Boogaarts, and G. Meijer, "Double-resonance spectroscopy on triplet states of CO," J. Mol. Spectrosc. **165,** 303–314 (1994).
32. N. Seiser and D. C. Robie, "Pressure broadening in the oxygen $b\ ^1\Sigma_g^+\ (v' = 1) \leftarrow X\ ^3\Sigma_g^-\ (v'' = 0)$ band measured by cavity ring-down spectroscopy," Chem. Phys. Lett. **282,** 263–267 (1998).
33. R. Engeln, G. von Helden, G. Berden, and G. Meijer, "Phase shift cavity ring down spectroscopy," Chem. Phys. Lett. **262,** 105–109 (1996).
34. D. Romanini, A. A. Kachanov, N. Sadeghi, and F. Stoeckel, "CW cavity ring down spectroscopy," Chem. Phys. Lett. **264,** 316–322 (1997).
35. B. A. Paldus, C. C. Harb, T. G. Spence, B. Wilke, J. Xie, J. S. Harris, and R. N. Zare, "Cavity-locked ring-down spectroscopy," J. Appl. Phys. **83,** 3991–3997 (1998).
36. S. L. Bragg, J. W. Brault, and W. H. Smith, "Line positions and strengths in the H_2 quadrupole spectrum," Astrophys. J. **263,** 999–1004 (1982).
37. D. W. Ferguson, K. N. Rao, M. E. Mickelson, and L. E. Larson, "An experimental study of the 4-0 and 5-0 quadrupole vibration rotation bands of H_2 in the visible," J. Mol. Spectrosc. **160,** 315–325 (1993).
38. L. A. Guildner, D. P. Johnson, and F. E. Jones, "Vapor pressure of water at its triple point," J. Res. Natl. Bur. Stand. **80,** 505–521 (1976).